6.1   GLOBAL SOLAR RADIATION IN A SOUTHERN AFRICAN SAVANNA ENVIRONMENT

M. Nasitwitwi [1,*], W. G. Bailey [2], and L. J. B. McArthur [3]

1. Department of Geography, Douglas College, New Westminster, British Columbia, V3L 5B2
2. Department of Geography, Simon Fraser University, Burnaby, British Columbia, Canada, V5A 1S6
3. Experimental Studies Division, Meteorological Service of Canada, Downsview, Ontario, Canada, M3H 5T4

1.0 Introduction

A pervasive dearth of radiation knowledge exists in Africa, with Zambia being a typical case. Amongst the radiation budget components, global solar radiation has in past years assumed economic importance as a renewable energy alternative (Lewis, 1981; World Solar Programme, 1999; Omran, 2000). More recently, global solar radiation is being studied due to its importance in providing energy for the earth's climate system.

National weather networks throughout Africa, have not routinely observed radiation fluxes because of the high cost of instruments and poor funding for the Meteorological Departments. In Zambia, this situation has been compounded by a severe attrition of qualified personnel to other countries; apathy amongst the scientific community towards atmospheric research; and an absence of local training facilities by which to develop a radiation cadre (United Nations Educational Scientific and Cultural Organization, 2001). Consequently, only a short monthly archive of global solar radiation measured at several Zambian stations between 1977 and 1983 forms the basis of Zambian literature published by Mwangala and Mukambulo (1980), Jain (1983) and Jain and Jain (1988). Fragmentary measurements were continued for a number of years, but have not been published because their reliability was strongly questioned (Lewis, 1981). Recent measurements of global solar radiation in western Zambia have

---

[*] Corresponding author address: M. Nasitwitwi, Department of Geography, Douglas College, New Westminster, BC Canada V3L 5B2; e-mail address: nasitwitwim@douglas.bc.ca

described dry season effects of aerosols (Eck *et al.*, 2001; Holben *et al.,* 2001; Schafer *et al.* 2002) as a result of anthropogenic biomass burning over the rural landscape (Desanker *et al.*, 1997; Scholes *et al.*, 1996).

Angstrom-type empirical radiation models based on sunshine hours were earlier utilized to provide radiation data in Zambia without validation against actual measurements (Spain, 1971). Subsequent work refined this model using Zambian data (Mwangala and Mukambulo, 1980; Jain, 1983; Jain and Jain, 1988). Further, Jain and Jain (1988) proposed regional coefficients of the Angstrom-type radiation model applicable to all Zambian locations. Errors in all these modelling procedures were due largely to the low accuracy of radiation and sunshine instrumentation. In addition, Jain and Jain (1988) isolated substantial unsystematic scatter of regression parameters of the Angstrom model indicative of physical atmospheric processes that were beyond the resolution of Angstrom's model.

Being tropical, the Zambian savanna ecosystem experiences three seasons: a warm-wet season from December to March; a cool-dry season from April to July; and a hot-dry season from August to November (Archer, 1971). This ecosystem, locally known as *miombo*, is characterized by annual bushfires from August to October, which generate substantial amounts of aerosols seasonally (Desanker *et al.*, 1997; Scholes *et al.*, 1996).

This paper discusses the properties of global solar radiation at Lusaka, Zambia measured over a wide range of meteorological conditions. Houghton's radiation model, which has a tradition of studying

urban aerosols and cloud effects in mid-latitude environments, is applied to a savanna landscape characterized by tropical atmospheric dynamics and pyrogenic aerosols produced by anthropogenic biomass burning. The model is used to determine the radiative influence of aerosols and other atmospheric controls on cloudless-sky global solar radiation regimes in savanna environments.

2.0 Theory

The sun emits electromagnetic energy in the wavelength range 0.1 to 4 μm. Extraterrestrial solar radiation (K_{ex}) incident at the top of the atmosphere is determined by solar output, sun-earth positioning, latitude, time of the year and time of the day such that

$$K_{ex} = I_o \cos Z\, E_o \qquad (1)$$

where I_o is the solar constant, Z is the solar zenith angle and E_o is the eccentricity correction factor of the earth's orbit.

Between the top of the atmosphere and the earth's surface, the atmosphere reflects, absorbs and scatters the incoming solar beam. The flux at the earth's surface, termed global solar radiation, is the sum of the direct-beam and the diffuse components. Assuming that multiple reflections between the surface and the atmosphere are non-existent, global solar radiation $K\downarrow$ is

$$K\downarrow = t\, K_{ex} \qquad (2)$$

where t is the clearness index.

When the direct beam from the sun penetrates the cloudless atmosphere, its intensity is reduced by scattering in which there is an angular redistribution of the energy and by absorption in which the energy is converted into either heat or photochemical change. Probability of non-interference of the incoming beam by the atmosphere is called transmittance. In the broadband spectrum from 0.1 to 4 μm wavelengths,

total cloudless-sky transmission is the product of transmissions due to water vapour absorption Ψ_{wa}, aerosol absorption Ψ_{da}, water vapour scattering Ψ_{ws}, Rayleigh scattering Ψ_{rs}, and aerosol scattering Ψ_{ds} (Houghton, 1954; Davies et al., 1975). Houghton's (1954) parameterization assumes that absorption of the solar beam occurs before scattering; half of dust depletion is due to absorption; and that absorption due to ozone negligible (Davies et al., 1975). Direct-beam solar radiation transmitted after absorption and scattering is therefore defined as

$$S_o = I_o \cos Z\, E_o\, \psi_{wa}\, \psi_{da}\, \psi_{ws}\, \psi_{rs}\, \psi_{ds} \qquad (3)$$

Under cloudless conditions, the amount of diffuse solar radiation D_o reaching the earth's surface is defined as

$$D_o = I_o \cos Z\, E_o\, \psi_{wa}\, \psi_{da}\, \frac{\left(1 - \psi_{ws}\, \psi_{rs}\, \psi_{ds}\right)}{2} \qquad (4)$$

Therefore, global solar radiation under cloudless sky conditions $K\downarrow_o$ is the sum of the direct-beam solar radiation S_o and diffuse solar radiation D_o

$$K\downarrow_o = S_o + D_o \qquad (5)$$

$$K\downarrow_o = I_o \cos Z\, E_o\, \psi_{wa}\, \psi_{da}\, \frac{\left(\psi_{ws}\, \psi_{rs}\, \psi_{ds} + 1\right)}{2}. \qquad (6)$$

Parameterizations of various transmissions were computed as follows:

$$\psi_{da} = \psi_{ds} = 0.975^m \qquad (7)$$

$$\psi_d = \psi_{da}\, \psi_{ds} = K^m \qquad (8)$$

$$\psi_{ws} = 1 - 0.0225 wm \qquad (9)$$

$$\psi_{wa} = 1 - 0.077 wm^{0.3} \qquad (10)$$

$$\psi_{rs} = 0.972 - 0.08262m + 0.00933m^2 - 0.00095m^3 + 0.0000437m^4 \qquad (11)$$

where the dust factor k = 0.95, w is precipitable water (in cm) and m is optical air mass (Houghton, 1954; Davies *et al.*, 1975).

3.0 Experimental Procedure

From April to December 2000, K↓ was continuously measured at Lusaka, Zambia (15° 24′ S, 28° 19′ E, 1154m) using an Eppley PSP Precision pyranometer. The instrument was mounted on a levelled 1.5 m platform on a rooftop at University of Zambia and was calibrated at 2.74 μV/Wm^{-2} by the National Atmospheric Radiation Centre of Canada. A Campbell Scientific 21X datalogger measured signals at one-second intervals and stored one-minute averages. Constant daily zero offsets given by averages of one-minute means of K↓ recorded between zenith angles 102° (nautical twilight) and 108° (astronomical twilight) were used to correct the measurements.

One-minute K_{ex} values were computed from daily values of the sun declination and the equation of time. The solar constant of 1366.1 Wm^{-2} in accordance with the ASTM 460 standard of the U.S. Naval Observatory and an eccentricity correction factor from McCullough's (1968) were also employed. The one-minute K_{ex} values were subsequently summed into hourly and daily values.

Supplemental data obtained from the Zambian Meteorological Department at Lusaka City Airport included total cloud amount, dry and wet bulb temperatures, upper air soundings and horizontal visibility. Precipitable water was evaluated from midday radiosonde upper air soundings of pressure, temperature and relative humidity. A model of precipitable water w and near-surface dewpoint temperature T_d was used to interpolate for periods that lacked soundings as follows:

$$\ln w = 0.087\, T_d - 0.4963 . \tag{12}$$

Hourly visibility observations were converted to atmospheric turbidity following the procedure of MacClatchey and Selby (1972)

$$\beta = 0.55\alpha\left(\frac{3.91}{Vis} - 0.01162\right)\left[0.02472(Vis - 5) + 1.132\right] \tag{13}$$

where β is atmospheric turbidity, Vis is visibility (in kilometres) and α is the wavelength exponent equal to 1.3 (Iqbal, 1983).

Cloudless hours with Z $\leq$ 70° were analyzed by months to determine seasonal variations. Thus the Houghton model estimated hourly $K\downarrow_o$ in each month with hourly transmissions due to water vapour absorption and scattering derived from daily values of precipitable water. Rayleigh scattering was calculated as a function of pressure-corrected air mass (Iqbal, 1983). A constant dust factor k = 0.95 was used to pre-evaluate transmission due to dust scattering and absorption. The residual between this model and measured hourly $K\downarrow_o$ was subsequently used to derive non-constant dust factors for the period April to November 2000. Effects of precipitable water and dry molecular air were jointly determined by the shortfall between K_{ex} and the hourly cloudless model at k = 1. In turn, aerosol influences were obtained by subtracting the hourly cloudless model with a non-constant dust factor from the hourly cloudless model at k = 1. Differencing the hourly cloudless model with a non-constant dust factor from actual surface measurements provided the seasonal trend of cloud effects.

4.0 Results
4.1 *Seasonal radiation variability*

K_{ex} ranged between 26 MJm^{-2}d^{-1} in the cool-dry season and 41 MJm^{-2}d^{-1} in the warm-wet season (Figure 1) as a consequence of seasonally varying solar zenith angles. Daily K↓ values were moderate in the cool-dry season with greater variability at the season's onset. Higher daily values of K↓ occurred
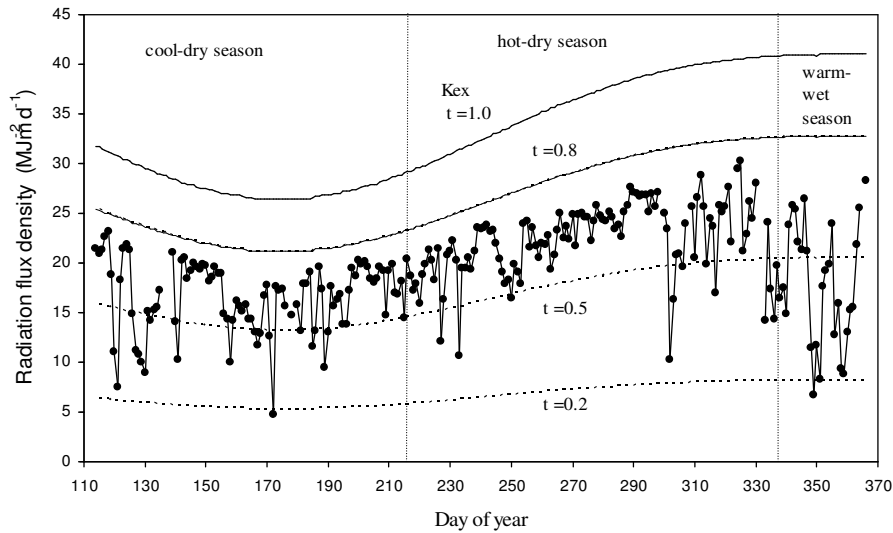
Figure 1. The trend of daily extraterrestrial radiation and global solar radiation for Lusaka, Zambia, April to December 2000. Reduction to extraterrestrial radiation as a consequence of clearness indices of 0.2, 0.5 and 0.8 is also denoted.

during the hot-dry season. A marked drop in the $K\downarrow$ trend and a more extreme day-to-day variability were observed at the onset of the warm-wet season. In proportion to K_{ex}, daily $K\downarrow$ was 0.2 - 0.7 in the cool-dry season; 0.5 - 0.7 in the hot-dry season; and 0.2 - 0.7 in the wet-warm season. This day-to-day variability of $K\downarrow$ was attributed mainly to cloud effects.

4.2 *Diurnal solar radiation regime*

Diurnal $K\downarrow$ varied closely with cloudiness, of which six classifications were identified. The distribution of diurnal radiation patterns and associated sky conditions across the seasons is given in Table1. Cloudless days typically presented absence of cloud cover with $K\downarrow$ symmetry centred on solar noon. These days mostly occurred in succession of each other under prevailing subtropical anticyclones (STACs) in the cool-dry and hot-dry seasons. Near-cloudless days also exhibited $K\downarrow$ symmetry around solar noon, but had limited cloud cover and noticeable fluctuation of $K\downarrow$ on a minute-by-minute basis. These days occurred in succession of each other and sometimes in combination with cloudless days under STACs. Cloud-free morning days typically comprised a cloudless morning, which degenerated into a cloudy afternoon when a threshold of approximately 800 Wm^{-2} of $K\downarrow$ was exceeded. This phenomenon was associated with convergence of the Congo air and northeasterly winds, which intensify afternoon turbulence (Hutchinson, 1974). On such days, the variation of $K\downarrow$ was large in the early afternoon. Cloud-free afternoon days consisted cloudy mornings that preceded cloudless afternoons. These may have resulted from Hutchinson's (1974) hypothesis that a secondary intensification of convection occurs at dawn due to radiative cooling which affects the Congo air and northeasterly winds. On cloudy days, $K\downarrow$ varied significantly due to transient cloud cover throughout the day, particularly at small solar zenith angles. Cloudy days were more frequent under the influence of the ITCZ. Very-cloudy days presented consistent cloud and low $K\downarrow$ caused by cloud opacity lasting all day. This therefore implied a greater fraction of diffused radiation on very-cloudy days.

Table 1. Clearness indices for the day type classifications for the cool-dry, hot-dry and warm-wet seasons for Lusaka, Zambia for April to December 2000.

Day type classification		Cool-dry season	Hot-dry season	Warm-wet season	All seasons
Cloudless days	No.	6	4	0	10
	Mean t	0.71	0.65		0.68
	Max t	0.74	0.71		0.74
	Min t	0.67	0.59		0.59
Near-cloudless days	No.	8	32	1	41
	Mean t	0.71	0.68	0.54	0.68
	Max t	0.74	0.75	0.54	0.75
	Min t	0.66	0.57	0.54	0.54
Cloud-free morning days	No.	35	44	1	80
	Mean t	0.66	0.64	0.62	0.65
	Max t	0.74	0.72	0.62	0.74
	Min t	0.49	0.51	0.62	0.49
Cloud-free afternoon days	No.	5	4	0	9
	Mean t	0.67	0.60		0.64
	Max t	0.73	0.68		0.73
	Min t	0.60	0.52		0.52
Cloudy days	No.	35	29	19	83
	Mean t	0.52	0.56	0.50	0.53
	Max t	0.68	0.67	0.69	0.68
	Min t	0.24	0.35	0.35	0.24
Very-cloudy days	No.	8	4	9	21
	Mean t	0.31	0.38	0.27	0.31
	Max t	0.38	0.49	0.39	0.49
	Min t	0.18	0.26	0.16	0.16

4.3 *Clearness Index*

Figure 2 shows the distinct seasonal pattern in t produced by effects of cloud cover, precipitable water and aerosols. Values of t in the cool-dry season ranged from 0.18 to 0.74. This range narrowed within 0.40 and 0.70 as the cool-dry season gave way to the hot-dry season. Variability in t increased in the hot-dry season, giving a seasonal range of 0.16 to 0.69. Overall, the daily t trend increased in the drier parts of the year, while it decreased in wet periods.

Typically, cloudless and near-cloudless days had high t values and the least variability. Overall, their mean was t = 0.68 with ranges of t = 0.15 and t = 0.21 respectively (Table 1). Cloud-free morning and cloud-free afternoon days had mean t values of 0.65 and 0.64, and ranges of 0.25 and 0.21 respectively. Cloudy days had a mean of t = 0.53 with a range of t = 0.44. Very-cloudy days had a mean t = 0.31 with a range of t = 0.33.
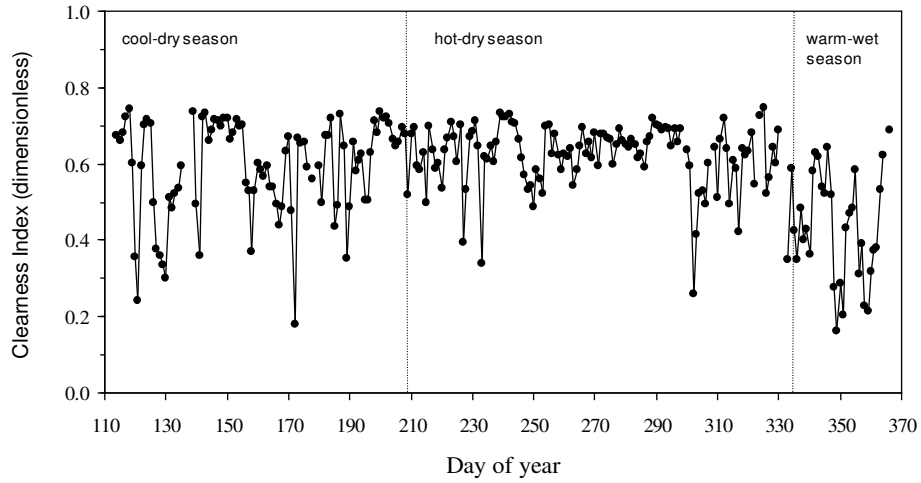
Figure 2. The trend of daily clearness index for Lusaka, Zambia, April to December 2000.

Monthly cumulative distributions of daily t are presented in Table 2. Wide-ranging clearness (0.1 < t < 0.7) was experienced in December, as it was a wet and cloudy month. The least variable sky conditions (0.4 < t < 0.7) occurred in September because it was a dry and generally cloudless month. This alternating pattern of sky conditions between dry and wet seasons was similar to those reported at other African savanna locations (Udo, 2000; Omran, 2000).

Table 2. Cumulative distribution frequencies of daily clearness indices for Lusaka, Zambia, April to December 2000.

Month	t 0.1	0.2	0.3	0.4	0.5	0.6	0.7	0.8	0.9	1.0	No of days
Apr	0.0	0.0	0.1	0.3	0.3	0.4	0.8	1.0	1.0	1.0	8
May	0.0	0.0	0.0	0.2	0.3	0.5	0.6	1.0	1.0	1.0	28
Jun	0.0	0.0	0.0	0.0	0.3	0.6	0.9	1.0	1.0	1.0	28
Jul	0.0	0.0	0.0	0.0	0.1	0.3	0.8	1.0	1.0	1.0	31
Aug	0.0	0.0	0.0	0.1	0.1	0.2	0.7	1.0	1.0	1.0	31
Sep	0.0	0.0	0.0	0.0	0.0	0.4	1.0	1.0	1.0	1.0	30
Oct	0.0	0.0	0.0	0.0	0.1	0.2	0.9	1.0	1.0	1.0	30
Nov	0.0	0.0	0.0	0.0	0.2	0.4	0.9	1.0	1.0	1.0	26
Dec	0.0	0.0	0.2	0.4	0.6	0.8	1.0	1.0	1.0	1.0	30

4.4 *Cloud effects*

Figure 3 uses percentage frequency distributions of hourly cloud cover in different months to highlight the seasonal pattern of cloudiness. Relatively clear sky conditions dominated from July to October due to STAC influences. April, May and November had more cloudiness due to convective activity induced by the ITCZ.

In Figure 4, a concave and inverse relationship between the hourly t values and hourly cloud cover was revealed. This suggested enhancement of $K\downarrow$ during low to medium cloudiness. The wide scatter in the regression resulted from varying transmissions of different cloud types.

4.5 *Atmospheric controls under cloudless skies*

The clearness index under cloudless skies t_o can be defined as

$$t_o = \frac{K\downarrow_o}{K_{ex}}. \tag{14}$$

Rayleigh scattering, aerosols, and water vapour scattering and absorption all control t_o at both the diurnal and seasonal scales. Rayleigh scattering in a dry molecular atmosphere is a function of pressure-corrected optical air mass m, which varies diurnally and annually. As m = sec Z for Z ≤ 70°, m is
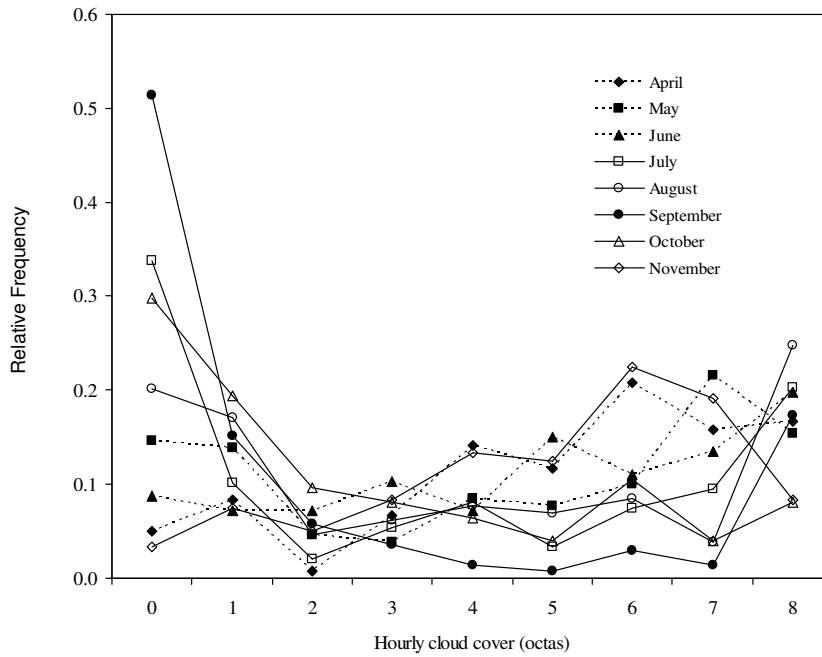
Figure 3. Frequency distribution of cloud amount for Lusaka, Zambia, April to November 2000.
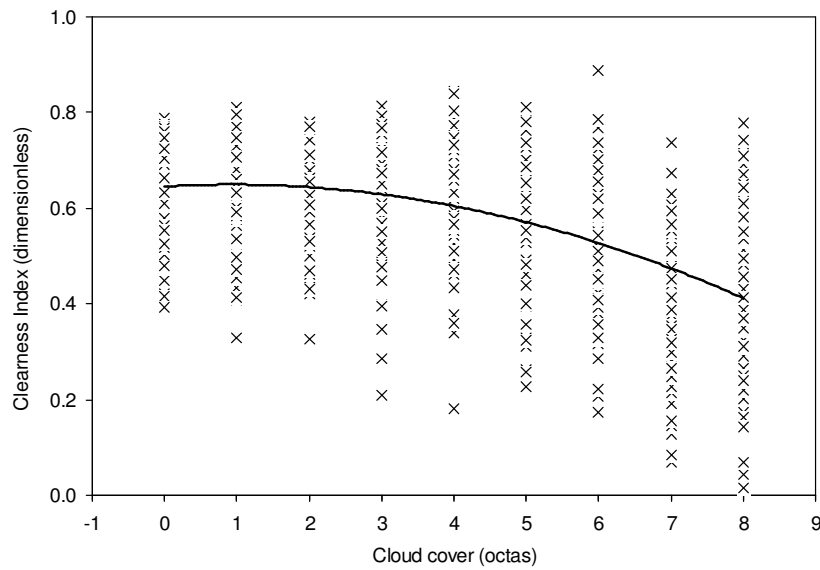

Figure 4. The relationship between hourly clearness index and cloud amount for Lusaka, Zambia, April to November 2000. The solid line is given by: $y = -0.0048\,x^2 + 0.0090\,x + 0.6452$, $r^2 = 0.3088$.

greatest under STACs in the cool-dry and hot-dry seasons because of larger zenith angles and higher atmospheric pressures. In Figure 5, daily precipitable water reduced under STAC conditions and increased as the ITCZ moved southward. In this study,

precipitable water did not seem to strongly affect t_o. Instead, low t_o values were associated with the dry season wherein precipitable water was minimal. This anomaly suggested an overriding radiative influence from aerosols.
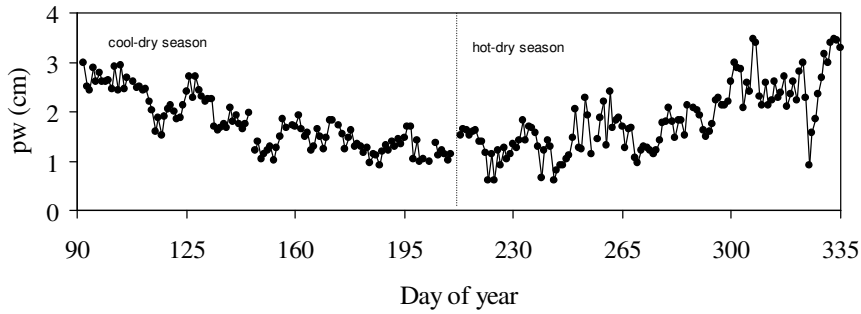
Figure 5. The trend in precipitable water for Lusaka, Zambia, April to November 2000.
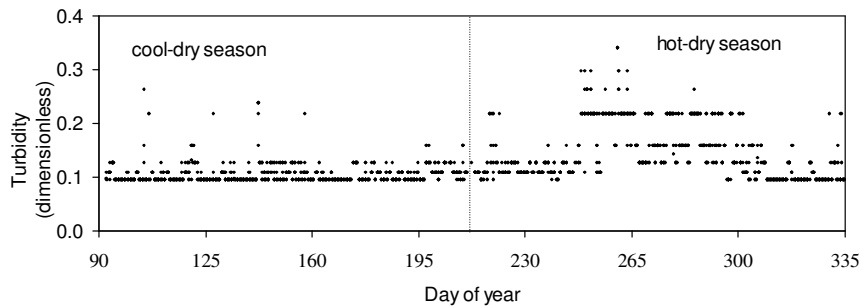

Figure 6. Hourly cloudless sky turbidity for Lusaka, Zambia, April to November 2000. The sample size is 2244 .

Hourly β values presented in Figure 6 indicated turbid conditions in the hot-dry season (β ~ 0.20) whereas the rest of the measurement period was virtually clear (β < 0.11). This increased turbidity coincided with extensive biomass burning and was compounded by limited vertical aerosol dispersion under STACs (Garstang et al., 1996). Consequently, the amount of $K\downarrow_o$ transmitted through these turbid atmospheres was greatly attenuated.

Regardless of zenith angle, a reduction in hourly t_o was observed with increased β (Table 3). Turbid atmospheres in the hot-dry season suffered depletion in t_o ranging between 10 to 13% in comparison to the off-season of biomass burning. This effect was attributable to high absorptivity of African savanna smoke such as observed by Eck et al. (2001) and Holben et al. (2001). The reduction of t_o by aerosols

in this study was lower than 22% reported by Schafer et al. (2002) because absolutely clean background values of β = 0.00 were not available.

4.6 *Model performance*

Ten completely cloudless days were observed, each with varying amounts of precipitable water and β values. Cloud free hours were isolated from cloudy days and also incorporated into the dataset for $K\downarrow_o$ modelling.

4.6.1. *Model performance on cloudless days*

Cloudless days varied when predicted and measured $K\downarrow_o$ were compared although the effects of a dry molecular atmosphere and water vapour were adequately simulated by pressure-corrected air mass and daily precipitable water respectively.

This lack of agreement between predictions and measurements resulted from seasonal changes in β. Between April and July, β was relatively low as the biomass burning was only beginning and hourly K↓$_o$ was well predicted by the model with K = 0.95 (Figure 7a). On such clear days, Houghton's dust parameterization was commensurate to the observed value of β = 0.10 with a slight overestimate. As β → 0.2 on more turbid days, model accuracy was reduced (Figure 7b) due to K↓$_o$ attenuation by biomass burning which occurred between August and November. Consequently, the model at k = 0.95 significantly overestimated the amount of K↓$_o$ during turbid sky conditions.

4.6.2. *Model performance in different seasons*

The hourly accuracy of Houghton's model varied according to prevailing atmospheric conditions in different seasons. Between April and June, low β values produced slight overestimates of K↓$_o$ and low mean absolute errors, mean bias errors and root mean square errors (Table 4). In this period, occasional rainfall cleaned out aerosols from the atmosphere; dust entrainment was inhibited by the presence of vegetation and soil moisture; and the fresh vegetation lacked the necessary fuel for fires.

Table 3. Dependence of hourly cloudless sky clearness index (t_o) on selected turbidities (β) and zenith angles (Z) for Lusaka, Zambia.

Turbidity	t_o for 30° ≤ Z ≤ 33°	t_o for 42° ≤ Z ≤ 45°
for β < 0.11	0.77 (0.8)	0.77 (2.0)[1]
	0.74 (0.8)	0.77 (1.5)
	0.74 (0.9)	0.76 (1.2)
	0.68 (0.9)	0.73 (1.4)
	0.65 (2.3)	0.71 (1.4)
	0.76 (1.9)	0.77 (1.0)
		0.77 (1.0)
		0.76 (1.0)
		0.76 (n/a)
		0.77 (n/a)
		0.74 (0.8)
		0.69 (0.8)
mean t	0.72	0.75
β > 0.20	0.60 (1.1)	0.59 (1.3)
	0.63 (1.5)	0.60 (1.2)
	0.64 (1.3)	0.73 (1.1)
	0.62 (1.3)	
	0.63 (1.2)	
	0.60 (1.2)	
mean t	0.62	0.64

1. bracketed values denote precipitable water (in cm)
2. n/a – not available

Table 4. Comparison of observed and predicted hourly cloudless-sky global solar radiation showing numbers of observations (n), observed means, predicted means, observed standard deviations, predicted standard deviations, mean absolute errors (MAE), mean bias errors (MBE), root mean square errors (RMSE) and indices of agreement (d) for Lusaka from April to December 2000. The value of d is dimensionless and the rest are in Wm^{-2}.

	n	Mean (o)	Mean (p)	s_o	s_p	MAE	MBE	RMSE	d
April	7	546	576	91	95	31	31	32	0.97
May	31	591	633	146	151	42	42	49	0.97
June	25	520	597	132	150	77	77	93	0.90
July	45	611	704	156	167	93	93	103	0.90
August	16	719	813	154	158	93	93	144	0.91
September	75	596	738	252	272	141	141	153	0.98
October	40	547	665	293	295	118	118	122	0.96
November	15	526	628	169	170	102	102	104	0.99
All	254	585	687	217	231	102	102	116	0.93

Errors of prediction increased as biomass burning intensified. A remarkable disparity between predictions and measurements was seen between August and October with $\beta > 3.0$. Biomass burning was possible at this time of the year because adequate fuel was available in the dry savanna vegetation. As biomass burning ceased around November, β values lowered and model accuracy improved.
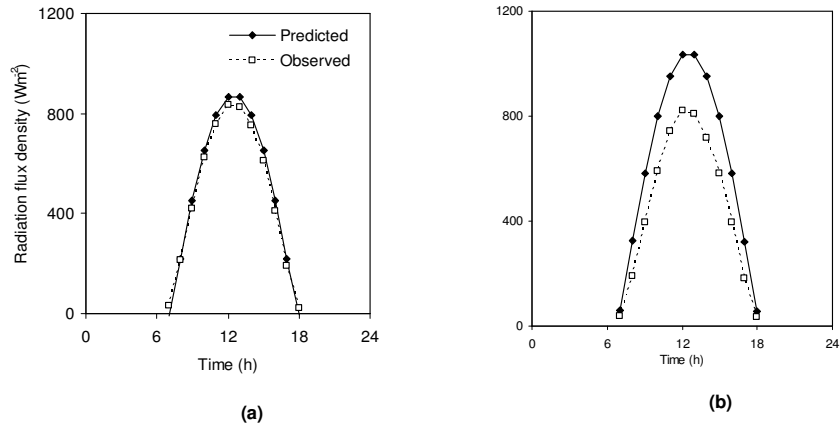
Figure 7. Predicted and observed cloudless-sky global solar radiation in Lusaka, Zambia on
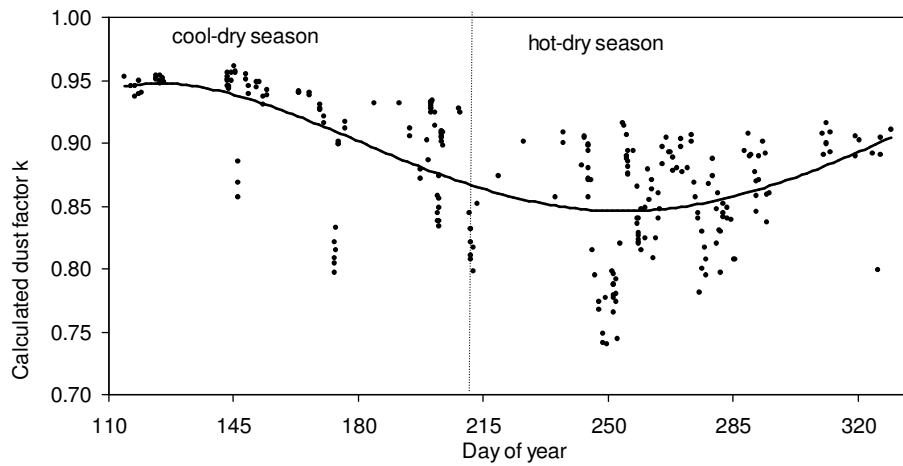(a) May 22, 2000 with turbidity at 0.1 and (b) on September 7, 2000 with turbidity at 0.2.

Figure 8. Calculated dust factor for cloudless hours at Lusaka, Zambia, April to
November 2000. The solid line is given by a polynomial.

4.6.3. *Calculation of transmissions from Houghton model*

Figure 8 shows that the original dust factor by Houghton (1954) practically exceeded all calculated k values. A wide variability was observed in the modelled dust factor with k ~ 0.95 at the beginning of the cool-dry season and $0.74 \leq k \leq 0.91$ in the hot-dry season. The lowest k values were recorded in the hot-dry season when biomass burning was at peak. The scatter in k increased as β increased.

Variable dust factors were hence employed to evaluate transmissions due to various atmospheric controls for different seasons of the savanna. The pattern of solar radiation due to seasonal changes in atmospheric attenuants is shown in Figure 9.
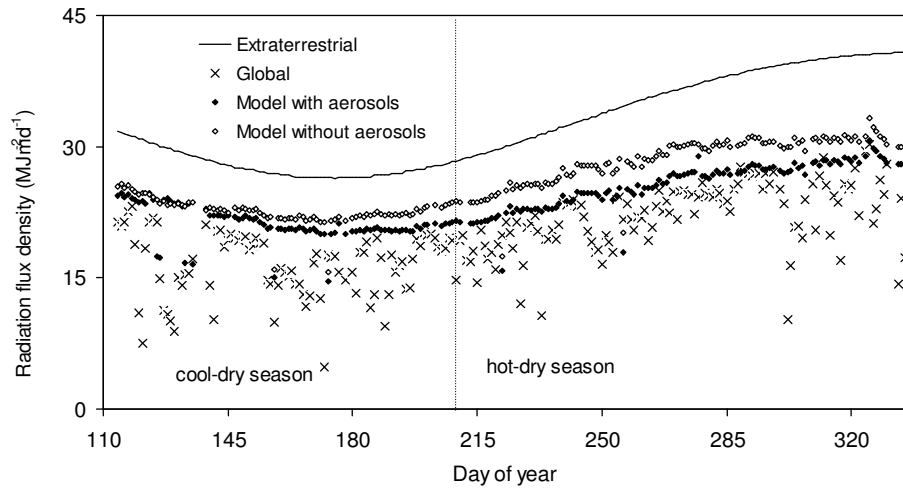
Figure 9. Extraterrestrial, observed and predicted global solar radiation with and wtihout aerosols at Lusaka, Zambia, April to November 2000.
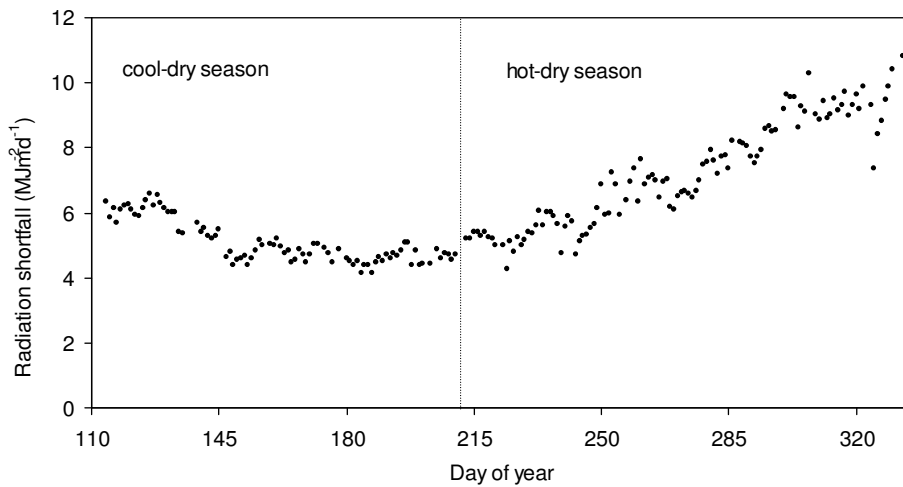

Figure 10. Shortfall of global solar radiation due to the combined effects of precipitable water and dry molecular air in Lusaka, Zambia, April to November 2000.

The combined effect of precipitable water and the dry molecular atmosphere resulted in losses of $K\downarrow$ ranging from 4 $MJm^{-2}d^{-1}$ in the cool-dry season to 11 $MJm^{-2}d^{-1}$ at the end of the hot-dry season. Generally, this effect was almost uniform for most of the cool-dry season but it steadily increased in the hot-dry season (Figure 10). Further this effect was greater when K_{ex} increased and the ITCZ moved into the Southern Hemisphere. Additional attenuation of K_{ex} was caused

by increased precipitable water under the ITCZ influence.

The shortfall of $K\downarrow_o$ due aerosol effects depicted a very pronounced seasonal trend although the shortfall due to aerosols is substantially less than that due to combined precipitable water and dry molecular air effects (Figure 11). It ranged from 1 $MJm^{-2}d^{-1}$ in the cool-dry season to 3 $MJm^{-2}d^{-1}$ in hot-dry season. A greater effect was observed in September where β
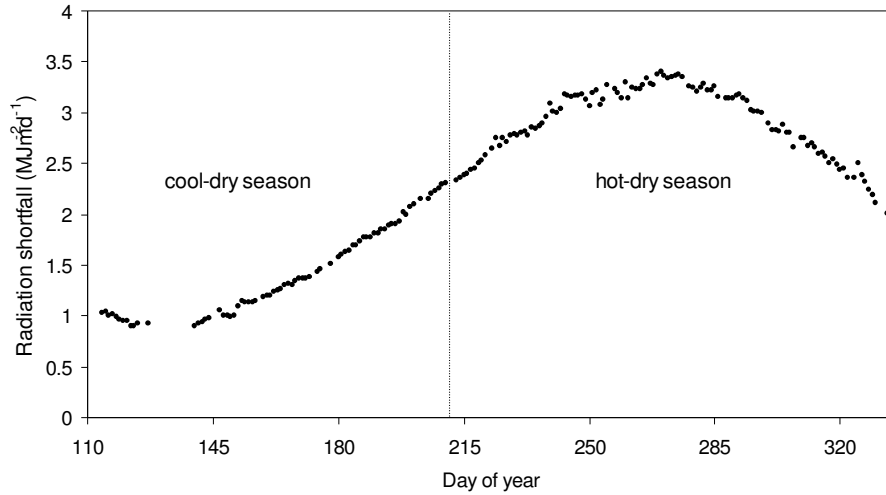
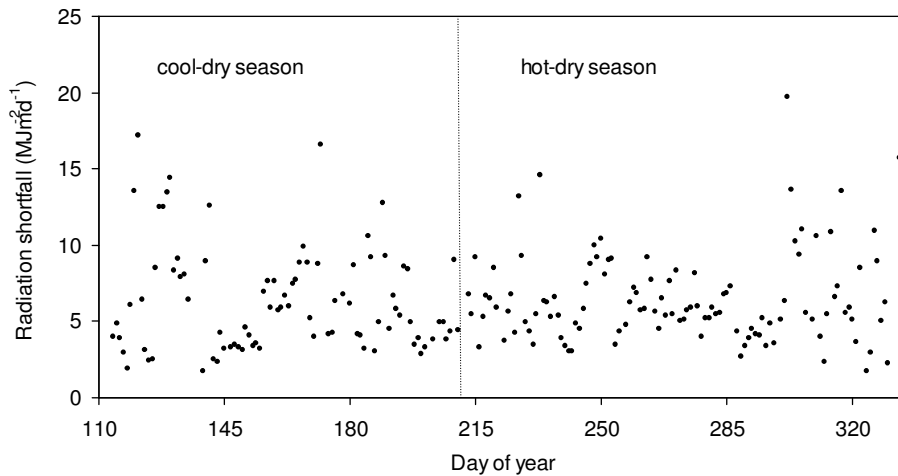Figure 11. Shortfall of global solar radiation due to aerosols at Lusaka, Zambia, April to November, 2000.

Figure 12. Shortfall of global solar radiation due to cloud effects in Lusaka, Zambia, April to November 2000.

was also highest. Thereafter, the loss of $K\downarrow_o$ due to aerosols began to reduce in the months of October and November. Overall, the shortfall of $K\downarrow_o$ was strongly associated with the increase in β due to biomass burning in the hot-dry season. Comparatively, the shortfall of $K\downarrow_o$ in the hot-dry season doubled over that in the cool-dry season. Measured reductions of $K\downarrow_o$ by Schafer et al. (2002)

are not significantly different from estimates by the Houghton model in this study.

Cloud effects did not show a very strong seasonality but in many cases outweighed the impacts of precipitable water, dry molecular air and aerosols (Figure 12). The shortfall of $K\downarrow_o$ varied widely from less than 2 $MJm^{-2}d^{-1}$ at the end of the hot-dry season to maxima of over 15 $MJm^{-2}d^{-1}$ that occurred both in cool-dry and hot-dry seasons. The

range is smallest around the middle of the hot-dry season reflecting cloudless conditions arising from subtropical anticyclones.

5.0 Conclusions

This paper characterized the $K\downarrow$ regime in the *miombo* savanna ecosystem of Zambia from the instantaneous to the seasonal temporal scales. The regional climate system via the ITCZ, the Hadley cell and the attendant STACs largely regulated the amount of $K\downarrow$ available at the surface. Moderate $K\downarrow$ amounts that were received in the warm-wet season were adequate to sustain seasonal vegetation production within this ecosystem. In the dry season, $K\downarrow$ amounts were abundant but vegetation production was inhibited by water deficits. The dry season $K\downarrow$ maxima therefore provide potential for a second crop in each year if affordable infrastructure for managing hydrological resources were developed to permit expanded irrigation during the dry season.

Conversely t variability reflected the inherent seasonality of the overall climate system and the importance of the associated cloud regimes. Localized anthropogenic activity (industrial activity, automobile emissions, etc.) around Lusaka, Zambia did not significantly attenuate $K\downarrow$ in non-burning periods of the year but biomass burning in the dry season doubled β values and caused a 10% shortfall in $K\downarrow$. Slash-and-burn agriculture is integral to the miombo savanna woodland ecosystem and may not pose "new" direct threats on future surface radiation climatologies at current agricultural levels. However, if slash-and-burn agriculture were either discouraged or expanded, with atmospheres becoming appreciably cleaner or more turbid respectively, changes in the future radiation regimes in southern Africa will arise in response. Concomitant changes to both the surface radiation and energy budgets will, out of necessity, ensue. Consequently, these regional forcings will impact the surface climates, and may be in distinct contrast to variation and changes that may arise from unrelated global processes and trends.

From comparisons between predicted and measured $K\downarrow_o$ under low and high β conditions, the hourly performance of Houghton's model was evaluated and the radiative forcing caused by atmospheric controls calculated. On clean and cloudless days with $\beta \sim 0.1$, the model closely approximated $K\downarrow_o$ because the dust factor $k = 0.95$ was commensurate with the relatively clean atmosphere. On turbid cloudless days with $\beta \sim 0.2$, the predictions by the model substantially overestimated $K\downarrow_o$ due to attenuation by an increased aerosol loading arising from biomass burning. Seasonally, the model tended to overestimate the amount of hourly $K\downarrow_o$ received because of the varying aerosol pattern in which the errors were largest at the peak of the biomass-burning period in September. The model of shortfalls of $K\downarrow_o$ due to atmospheric controls showed random effects by clouds ($2 - 15$ $MJm^{-2}d^{-1}$); a conservative effect by precipitable water and dry molecular air ($4 - 11$ $MJm^{-2}d^{-1}$); and highly seasonal effects by aerosols ($1 - 3$ $MJm^{-2}d^{-1}$). Previous Angstrom-type radiation models may have severely overestimated $K\downarrow$ incident in savanna ecosystems due to their failure to treat aerosol effects in the biomass-burning period. This situation necessitates all future estimations of $K\downarrow$ to explicitly account for the aerosol effects, which are an integral characteristic of the savanna atmospheres.

References

Archer, D. R., 1971: "Temperature, humidity, sunshine and winds" In Davies, D. H. (ed): Zambia in Maps, University of London Press, London, 22 – 23.

Davies, J. A., Schertzer, W., and Nunez, M., 1975: Estimating global solar radiation, Boundary-Layer Meteorology, **9**, 33 - 35.

Desanker, P. V., Frost, P. G. H., Frost, C. O., Justice, C. O. and Scholes, R. J., 1997: The Miombo Network: Framework for a terrestrial transect study of land-use and land-cover change in the miombo ecosystems of central Africa, IGBP Report 41, The International Geosphere-Biosphere Program (IGBP), Stockholm, 74 pp.

Eck, T F., Holben , B. N., Ward, D. E., Dubovik, O., Reid, J. S., Smirnov, A., Mukelabai, M. M., Hsu, N. C., O'Neill, N. T. O., and Slutsker, I., 2001: Characterization of the optical properties of biomass burning aerosols in Zambia during the 1997 ZIBBEE field campaign, Journal of Geophysical Research, **106**, 3425 – 3448.

Garstang, M., Tyson, P. D., Swap, R., Edwards, P., Kallberg, P., and Lindsay, J. A., 1996: Horizontal and vertical transport of air over southern Africa, Journal of Geophysical Research, **101(D19)**, 23721 – 23736.

Holben , B. N., Tanre, D., Smirnov, A., Eck, T F., Slutsker, I., Abuhassan, N., Newcomb, W. W., Schafer, J., Chatenet, B., Lavenue, F., Kaufman, Y. J., Vande Castle, J., Setzer, A., Markham, B., Clark, D., Frouin, R., Harthore, R., Karnieli, A., O'Neill, N. T., Pietras, C., Pinker, R. T., Voss, K., and Zorbi, G., 2001: An emerging ground-based aerosol climatology: Aerosol optical depth from AERONET, Journal of Geophysical Research, **106**, 12067 – 12097.

Houghton, H. G.,1954: On the annual heat balance of the Northern Hemisphere, Journal of Meteorology, **11(1)**, 1 - 9.

Hutchinson, P., 1974: The climate of Zambia, Zambia Geographical Association, Occasional Study No. 7, 95 pp.

Iqbal, M., 1983: An Introduction to solar radiation, Academic Press, Toronto, 391 pp.

Jain, P. C., 1983: Solar Irradiation in Zambia, Internal Report, International Centre for Theoretical Physics, Trieste, Italy, 26 pp.

Jain, S. and Jain, P. C., 1988: A comparison of Angstrom-type correlations and the estimation of monthly daily global irradiation, Solar Energy, **40(2)**, 93 -98.

Lewis, G., 1981: Irradiance estimates for Zambia, Solar Energy, **26**, 81-85.

MacClatchey, R. A. and Selby, J. E., 1972: Atmospheric transmittance from 0.25 to 38.5 μm: computer code LOWTRAN-2, Air Force Cambridge Research Laboratories, AFCRL-72-0745, Environ. Res. Paper 427.

McCullough, E. C., 1968: Total daily radiant energy available extraterrestrially as a harmonic series of the day of year, Arch. Meteor. Geophys. Bioklim., **B16**, 129 – 143.

Mwangala, S. and Mukambulo, N. K., 1980: Global, longwave and net radiation in Zambia, Technical Memorandum No. 10, Meteorological Department, Lusaka, Zambia, 13 pp.

Omran, M. A., 2000: Analysis of solar radiation over Egypt, Theoretical and Applied Climatology, **67**, 225 – 240.

Schafer, J. S., Elk, T. F., Holben, B. N., Artaxo, P., Yamasoe, M. A. and Procopio, P. S., 2002: Observed reductions of total solar irradiance by biomass burning aerosols in the Brazilian Amazon ans Zambian Savanna, Geophysical Research Letters, **29(17)**, 1 – 4.

Scholes, R. J., Ward, D. E. and Justice, C. O.,1996: Emissions of trace gases and aerosol particles due to vegetation burning in southern hemisphere Africa, Journal of Geophysical Research, **101(D19),** 23677 – 23682.

Spain, E. S., 1971: Calculated Radiation in Zambia, Climate Data Publication No. 16, Department of Meteorology, Lusaka, 21 pp.

Udo, S. O., 2000: Sky conditions at Ilorin as characterized by clearness index and relative sunshine, Solar Energy, **69(1)**, 45 – 53

United Nations Educational Scientific and Cultural Organization, 2001: Energy efficiency in Africa for sustainable development – Final Report, Nairobi, Republic of Kenya, 7 pp.

World Solar Programme, 1999: World Solar Programme 1996 – 2005: Africa (ASP) mechanisms for implementation (an outline), 19 pp.